

RESEARCH ARTICLE

Spatial Concordance of Tumor Proliferation and Accelerated Repopulation from Pathologic Images to 3'-[¹⁸F]Fluoro-3'-Deoxythymidine PET Images: a Basic Study Guided for PET-Based Radiotherapy Dose Painting

Chengming Li,^{1,2} Xiaoli Zhang,² Linlin Pang,² Yong Huang,³ Yongsheng Gao,⁴ Xindong Sun,² Jinming Yu,² Xue Meng²

¹School of Medicine and Life Sciences, University of Jinan-Shandong Academy of Medical Sciences, Jinan, China

²Department of Radiation Oncology, Shandong Academy of Medical Science, Shandong Cancer Hospital Affiliated to Shandong University, No 440, Jiyuan Road, Jinan, 250117, China

³Department of Nuclear Medicine, Shandong Academy of Medical Science, Shandong Cancer Hospital Affiliated to Shandong University, Jinan, China

⁴Department of Pathology, Shandong Academy of Medical Science, Shandong Cancer Hospital Affiliated to Shandong University, Jinan, China

Abstract

Purpose: To assess tumor cell proliferation and repopulation during fractionated radiotherapy and investigate the spatial concordance of cell proliferation and repopulation according to the uptake of 3'-[¹⁸F]fluoro-3'-deoxythymidine ([¹⁸F]FLT).

Procedures: Mice bearing A549 xenograft tumors were assigned to five irradiated groups, including 3 fraction (f)/6 days (d), 6f/12d, 9f/18d, 12f/24d, and 18f/36d with 2 Gy/f irradiations performed every other day and one non-irradiated group. Serial [¹⁸F]FLT positron emission tomography (PET) scans were performed at different time points as the groups finished the radiotherapy. The maximum of standard uptake values (SUVmax) were measured to confirm the likely time of tumor repopulation. A layer-by-layer comparison between SUVmax of PET images and Ki-67 LI of pathology images, including the thresholds at which maximum overlap occurred between FLT-segmented areas and cell proliferation areas were conducted to evaluate the spatial correlation.

Results: The SUVmax decreased in the 3f/6d group ($P=0.000$) compared to the non-irradiated group, increased in the 6f/12d group and then gradually reduced with prolonged treatment. Proliferation changes in 6f/12d group on pathology images were also confirmed. Significant correlations were found between the SUVmax and Ki-67 LI in each *in vitro* tumor of cell proliferation group and accelerated repopulation group (both of the $P<0.001$). Furthermore, the mean overlap region rates (ORRs) were 56.21 % and 57.82 % in the proliferation group and repopulation group, respectively. The data represented the preferable registration.

Conclusions: [¹⁸F]FLT PET is a promising imaging surrogate of tumor proliferative response to fractionated radiotherapy and may help make an adaptive radiation oncology treatment plan to realize radiotherapy dose painting.

Key words: [¹⁸F]FLT PET/CT, Non-small cell lung cancer, Tumor accelerated repopulation, Spatial concordance, Radiotherapy dose painting

Introduction

The prognosis of patients with locally advanced non-small cell lung cancer (NSCLC) remains poor despite the use of new radiation techniques and addition of chemotherapy to radiotherapy [1–3]. Poor overall survival with chemoradiotherapy is related to sufficient local tumor control despite distant metastases. Increasing the radiation dose may improve local control, but the risk of complications will limit the possibility of dose escalation. The target volume is one of the critical factors that has an impact on dose escalation. Therefore, a more sophisticated approach may be to selectively increase the dose to treatment-resistant areas while maintaining the dose to other parts of the target volume instead of escalating the dose to the whole tumor, which is called dose painting [4]. This requires an imaging biomarker to determine more treatment-resistant sub-volumes that should receive a higher dose. Functional imaging can complement anatomic imaging modalities and provide biologic tumor information relevant to radiotherapy dose planning by selecting the appropriate PET tracer [5].

The development of 3'-[¹⁸F]fluoro-3'-deoxythymidine ([¹⁸F]FLT) as a PET tracer has enabled *in vivo* demonstration of cell proliferation [6]. In the field of radiation oncology, [¹⁸F]FLT PET may be used potentially in patient selection for treatment modification based on the tumor proliferation and identification of tumor sub-volumes with a high density of actively proliferating cells amenable to increased dose. Accelerated repopulation of tumor cells during the course of radiotherapy is a common phenomenon in many kinds of cancers that affects radiation outcome [7, 8]. However, the question of when an imaging surrogate should be used for evaluating NSCLC proliferation during radiotherapy remains a concern. In addition, the spatial distribution of the tracer within the tumor tissue is obviously affected by the chaotic nature of tumor vascularization and irregularities of blood flow [9]. Correspondingly, the first and essential step for [¹⁸F]FLT to be applied in image-guided dose-painting is the *in vivo* demonstration of a spatial concordance between the pattern of intratumoral [¹⁸F]FLT uptake and the spatial pattern of its biologic target, which can be imaged with histopathologic or immunohistopathologic techniques. Threshold-based approaches may provide an alternative and a more intuitive mean to analyze the spatial concordance between the pattern of [¹⁸F]FLT uptake and cell proliferation in images from tissue specimens.

Therefore, the first aim of this study was to identify sub-volumes with a high density of tumor cell proliferation and accelerated repopulation at the time points of before and, more importantly, during radiotherapy based on [¹⁸F]FLT

PET. The second aim was to investigate the spatial concordance between the pattern of intratumoral uptake [¹⁸F]FLT and the spatial distribution of cell proliferation markers at the time point of tumor cell proliferation and repopulation, respectively.

Materials and Methods

Experimental Design

Human lung adenocarcinoma cell line (A549) obtained from the Chinese Academy of Sciences Shanghai Institute of Cell Bank was used to establish tumor xenografts in 6- to 8-week-old female BALB/c nude mice from the right thigh subcutaneous inoculation of 2×10^6 cells/site. In our previous study [10], we found that the repopulation could happen in the group irradiated every other day. The most common dose in clinical practice is 2 Gy/fraction (f). The tumor-bearing mice were randomly divided into five different irradiated groups, including 3f/6 days (d), 6f/12d, 9f/18d, 12f/24d, and 18f/36d, with 2 Gy/f irradiation every other day and one non-irradiated group to determine non-treatment cell proliferation, when the tumors reached 8–10 mm in diameter. Animal maintenance and all experimental procedures were carried out according to the protocol approved by the Chinese animal welfare regulations.

To detect the best time of tumor-accelerated repopulation based on [¹⁸F]FLT PET during irradiation, the first set of experiments was performed. In the non-irradiation group, micro-PET scans were performed just when the tumor reached 8–10 mm. Considering the proliferation after radiotherapy will reduce with time, the PET scans were acquired at the same interval time from the ending of radiotherapy in different groups. Then, tumors were excised and the immunohistochemical findings were performed to confirm the tumor-accelerated repopulation.

To investigate the spatial concordance between the pattern of intratumoral uptake [¹⁸F]FLT and the spatial distribution of cell proliferation markers, the second set of experiments was conducted. The tumor cell proliferation group and tumor-accelerated repopulation group selected by the first step underwent micro-PET. Then, tumors were excised and immediately placed on the tumor-marker-holder using the methodology for co-registration of histopathologic and autoradiography images. After scanning, the immunohistochemistry was performed for the spatial concordance of cell proliferation and accelerated repopulation.

Micro-PET Imaging and Analysis

Mice were injected with [¹⁸F]FLT at a median activity of 4.37 MBq (range, 0.68–5.01 MBq) *via* the tail vein. The procedures of images acquisition were as described previously [10]. Mice were euthanized immediately after *in vivo* micro-PET/CT scanning was finished, and the tumors were removed with no other tissue residue. To make sure the autoradiography and microscopy images were co-registered, we used an *in vitro* tumor-marker-holder made by the three-dimensional printing technology (Fig. 1). Then, the tumor was fixed to the holder and underwent *in vitro* PET/CT scanning in the same way as *in vivo* PET/CT scanning. According to the low-density crisscross on the CT images, the layer just where the passageway of the threads went through was selected as reference (Fig. 2).

Semi-quantitative analysis was performed using the standardized uptake value (SUV). The region of interest (ROI) was used to calculate the maximum SUV (SUV_{max}) by taking the ratio of maximal tracer uptake in the ROI to the injected activity normalized to body weight.

Immunohistochemistry Studies

After tumors were fixed overnight in 10 % formalin and embedded in paraffin blocks, several stacks of consecutive tissue sections of 4-um thick were obtained for immunohistochemical staining. To measure tumor proliferation, slides were incubated with mouse monoclonal antibodies against Ki-67 MIB-1 (dilution 1:200; Dianova; Hamburg; Germany). For Ki-67 staining, five non-overlapping fields of non-necrotic areas were selected in each ROI. The fraction of Ki-67 was assessed by examination of stained sections at

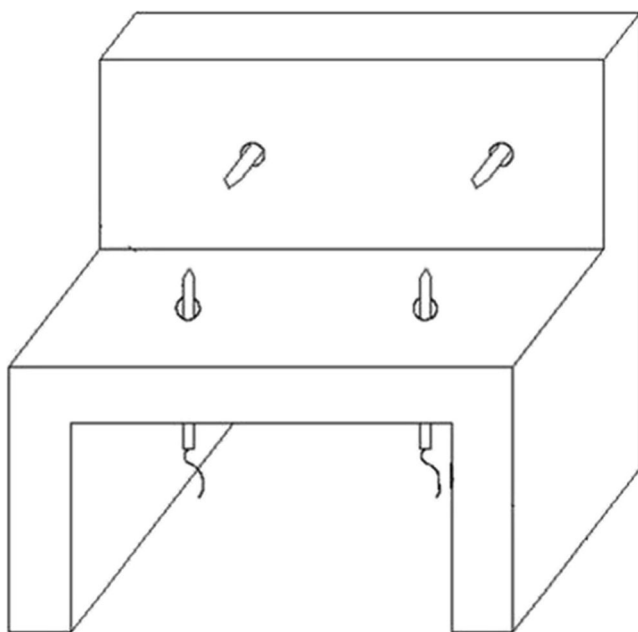


Fig. 1. The tumor-marker-holder.

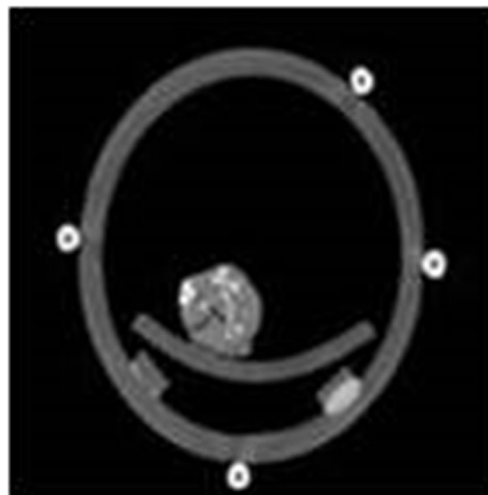


Fig. 2. The layer of the low-density crisscross on the CT images, where the passageway of the threads was selected as reference.

×400 magnification. The Ki-67 LI was calculated as the total number of Ki-67 positively stained cells of all five fields divided by 1000 (200 cells in each field). All samples were blinded for analysis.

Registration and Analysis from Pathologic Images to PET/CT Images

The CT and microscopy images were co-registered using the crisscross passageway on CT and pathology images, respectively. The collimation and interval of CT and PET scanning are described in Fig. 3. Thereafter, the A1 layer of PET scanning was the a1 layer of CT scanning and the P1/P2 layer of specimens. In addition, the A3 layer of PET scanning was just the a6 layer of CT scanning and the P5/P6 layer of specimens. Thus, all odd layers of PET images and corresponding pathological sections were selected for data analysis in the next step.

A rectangular coordinate system was set up in the PET image and the corresponding Ki-67-staining image respectively to evaluate the spatial relationship between the autoradiography and microscopy images. A quantitative co-registration between these two images was built according to the scale on the *x* and *y*-axes. All the areas were evaluated using the number of the small grids in the rectangular coordinate system. Four ROIs numbered 1–4 were randomly outlined without overlap in every selected layer of PET images as well as the corresponding layer of odd pathological sections. Overlap region rate (ORR) was cited to evaluate the relationship between the high proliferative region (HPR) in PET images and the HPR in the homologous pathological images. The ORR was defined as a ratio of the overlapping area divided by the total area: $\text{ORR} = \frac{\text{HPR}_{\text{pet}} \cap \text{HPR}_{\text{path}}}{\text{HPR}_{\text{pet}} \cup \text{HPR}_{\text{path}}}$. The 80 % SUV_{max} was used as the high uptake

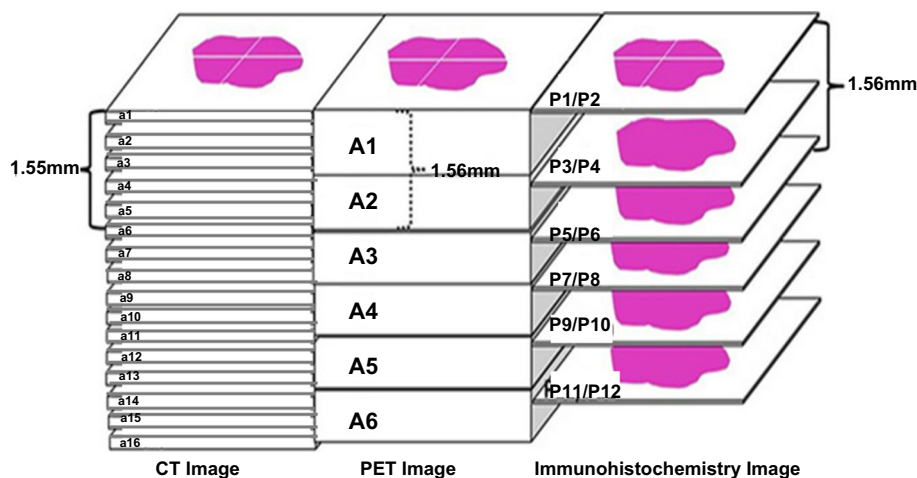


Fig. 3. The registration of [^{18}F]FLT PET/CT images and pathological images. The thickness of five CT layers (1.55 mm) was similar with two PET layers (1.56 mm). The pathological section thickness was 4 μm , and two sequence pathological sections as the same layer were considered to have one to one correspondence to the same PET layer. Considering the layer thickness of PET scanning was 0.78 mm, the two consecutive layers of pathological specimens were also cut at an interval of 0.78 mm. The A1 layer of PET scanning was the a1 layer of CT scanning and the P1/P2 layer pathological specimens, and the A3 layer of PET scanning was the a6 layer of CT scanning and P5/P6 layer of specimens.

region [11] to automatically delineate the HPR with the PMOD software in PET image (HPR_{PET}). In addition, the HPR in pathological image (HPR_{path}) was defined as regions where the Ki-67 LI $\geq 80\%$, using the in-house software tool developed with MoticDSAssistant Lite (version R2013a; MathWorks, Natick, MA).

Statistical Analysis

Statistical analysis was performed with SPSS software, version 17.0 (SPSS Inc.). All data were expressed as the mean \pm standard deviation (SD). The Kolmogorov-Smirnov test was used to evaluate the Gaussian distribution. The differences between the uptake of FLT PET and Ki-67 LI among different groups were analyzed with one-way ANOVA followed by the Bonferroni post hoc test. The Ki-67 LI and FLT uptakes were compared using linear regression analysis. All statistical tests were two-sided and performed at a 5 % level of significance.

Results

The Feasible Time Points of Tumor Cell Proliferation and Accelerated Repopulation Based on [^{18}F]FLT PET

A total of 26 mice (4–5 for each fractionation group and 5 in the non-irradiated group) completed PET scans and tumor excision for the first set of experiments. Four mice died from cachexia, so their tumors were not evaluated.

The average SUVmax of non-irradiated tumors was 2.0343. Compared to the SUVmax for non-irradiated tumors, decreases were observed in the 3/6d group (1.4399, $P=0.000$). However,

SUVmax was significantly increased later in the 6f/12d group when compared to the 3f/6d group (2.3327, $P=0.000$); however, this difference was not significant when comparing to the non-irradiated group ($P=0.056$). Then, SUVmax gradually decreased with prolonged treatment time (Fig. 4a), and the average value of 9f/18d group, 12f/24d group, and 18f/36d group was 1.5112, 1.5812, and 0.9782, respectively. Proliferation changes during fractionated radiotherapy were confirmed (Fig. 4b). The mean Ki-67 LI of non-irradiated tumors was 79.82 %, while it was 78.47 % in the 3f/6d group ($P=0.265$). After irradiation, Ki-67 LI in the 6f/12d group was significantly increased from 3f/6d group (82.33 %, $P=0.006$), it decreased with prolonged treatment time in both 12f/24d and 18f/36d groups (both of the $P=0.000$). Furthermore, strong correlations were found between Ki-67 LI and SUVmax ($r=0.836$, $P=0.001$). A plot of the correlation can be seen in Fig. 5.

The Spatial Concordance between the Pattern of [^{18}F]FLT Uptake and the Spatial Distribution of Cell Proliferation Markers at the Time Point of Tumor Cell Proliferation and Accelerated Repopulation

There was a total of nine mice, including five of the non-irradiated group and four of 6f/12d group, which were the tumor cell proliferation group and accelerated repopulation group, respectively. From the CT scanning images of all mice in the two groups, the crisscrossed passageway of the threads was observed. Then, all the *in vitro* tumors were cut into three segments following the two parallel layers confirmed by threads, except for the no. 2 tumor in the non-irradiated group which was cut into two segments. The CT and microscopy images were co-registered by the exhibited crisscross passageway on PET/CT and pathology

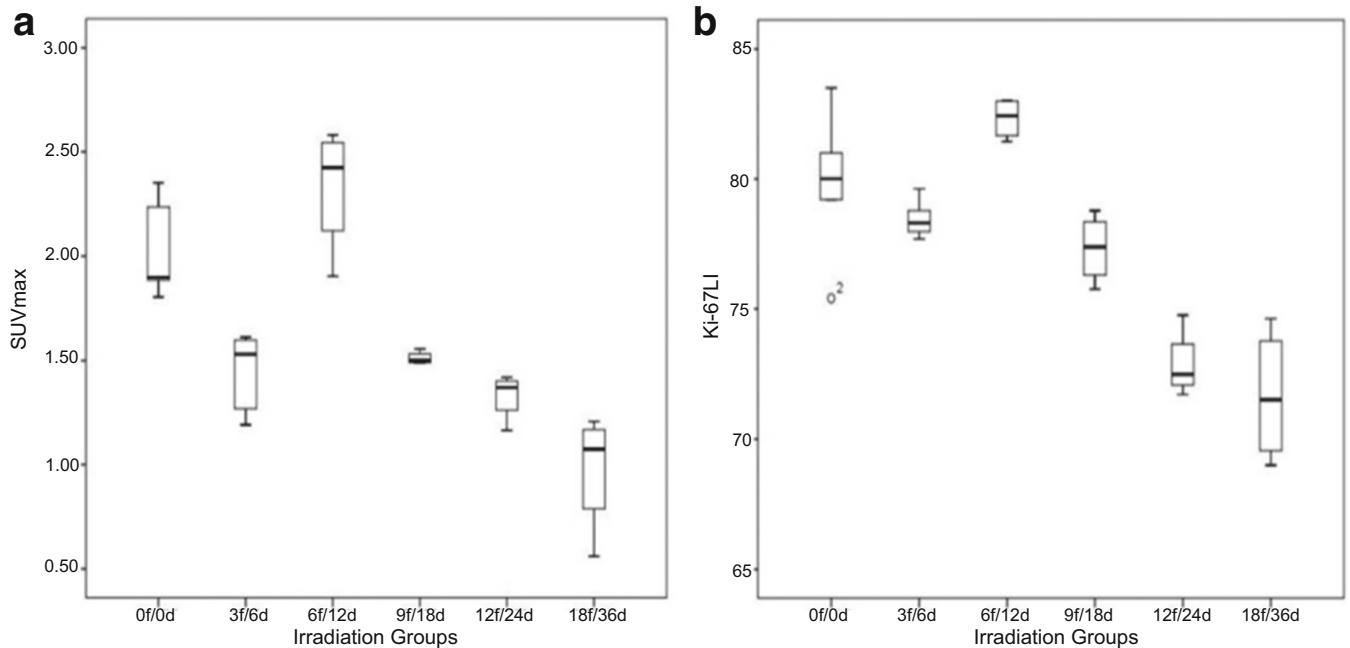


Fig. 4. **a** Dose-response trend in different irradiation groups with the SUVmax. **b** Dose-response trend in different irradiation groups with Ki-67 LI.

images, respectively. Four to six layers of PET/CT images and the same layers of pathologic specimens were selected for analysis in each tumor. Correspondingly, a total of 25 PET/CT image layers and the same layers of 50 pathologic sections in tumor cell proliferation group, as well as 22 PET/CT image layers and 44 pathologic sections in accelerated repopulation group were analyzed.

Four ROIs were outlined randomly without overlap by the rectangular coordinate system using the MoticDSAssistant Lite on every selected layer of PET image as well as the corresponding layer of odd pathologic section. Significant correlations were found between the SUVmax and Ki-67 LI of all ROIs in each *in vitro* tumor of the cell proliferation group and repopulation

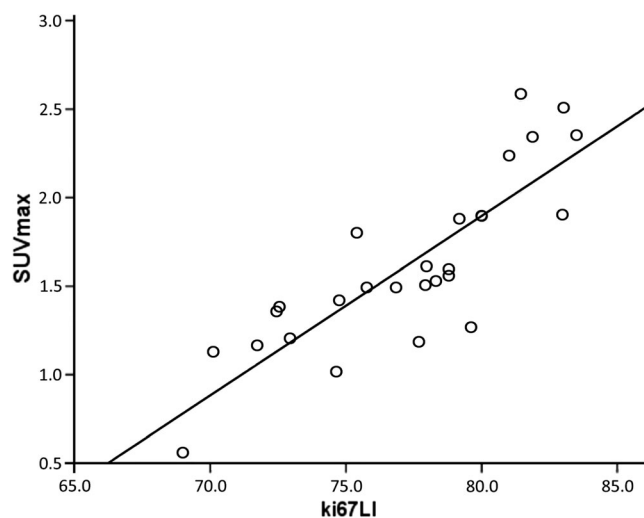


Fig. 5. A plot of the correlation between FLT uptake and Ki67 LI.

group (both of $P < 0.001$). Regions of high-intensity [¹⁸F]FLT uptake in the autoradiographs were observed to exhibit prominent staining for Ki-67. For example, in the no. 3 tumor in 6f/12d group, the SUVmax of randomized ROIs numbered 1–4 on the layer of A3 PET image were 1.4167, 1.7371, 1.8371, and 2.2355, respectively, and the Ki-67 LI of the corresponding ROIs on the same layer of P6 pathologic section was 58 %, 70 %, 78 %, and 94 %, respectively (Fig. 6a–d).

Furthermore, the ORR was calculated to evaluate the relationship between the HPR in selected layers of PET images and HPR in the same layers of the pathological specimens (Fig. 6e–f). Then, overlap comparisons of spatial location between PET and pathological sub-volumes were also performed on 25 PET/CT and pathology image layers in the proliferation group and 22 image layers in repopulation group, respectively. The mean ORR was 56.21 ± 12.81 % (range 31.43 %–81.67 %) in all layers of the tumor cell proliferation group. Comparing the mean ORR in the other layers of PET and corresponding pathology images, the mean ORR of 64.25 ± 8.8 % (range 50.63 %–81.67 %) was significantly higher in the A1 layers of PET and P2 pathology images in each segment of all tumors ($F = 12.567$, $P = 0.000$). Furthermore, using the same exhibited lesion of crisscross passageway as reference, the ORRs in both A1 layers of PET imaging between segments 1 and 2 in each tumor were very close except for the no. of tumor 1 (Table 1).

Similar results were also found in the 6f/12d group. The mean ORR was 57.82 ± 4.82 % (range 47.06 %–63.83 %) in all layers. Comparing the mean ORR in the other layers of PET and the corresponding pathology images, the mean ORR of 60.63 ± 3.0 % (range 53.19 %–63.83 %) was also significantly higher in the A1 layers of PET and P2 pathology images in each segment of all

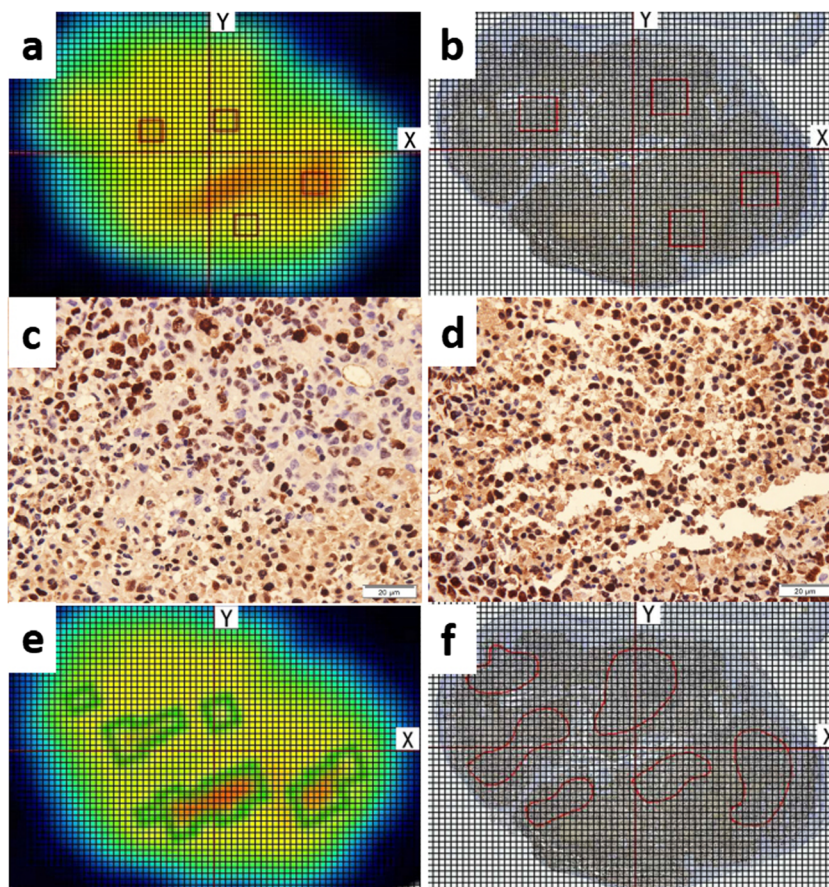


Fig. 6. **a** Four randomized ROIs on a layer of PET images, numbered 1 to 4 from the highest uptake to the lowest uptake; **b** corresponding 1–4 ROIs on the same layer of the pathologic section (H&E, $\times 10$); **c** and **d** amplified pathologic images from the regions numbered 1 and numbered 4 (H&E, $\times 400$); **e** and **f** overlap of spatial location between PET and pathological subvolumes.

Table 1.. The ORR of high proliferative region between PET and corresponding pathology image in 0f/0d

Tumor	Segment no.	PET layer no.	Path section no.	$HPR_{pet} \cap HPR_{path}$	$HPR_{pet} \cup HPR_{path}$	ORR (%)
1	1	A1	P2	49	60	81.67
	1	A3	P6	38	72	52.78
	2	A1	P2	45	70	64.29
	2	A3	P6	46	88	52.27
2	3	A1	P2	48	82	58.54
	1	A1	P2	46	76	60.53
	1	A3	P6	31	60	51.67
	2	A1	P2	45	76	59.21
	2	A3	P6	42	78	53.85
3	1	A1	P2	38	54	70.37
	2	A1	P2	42	63	66.67
	2	A3	P6	23	47	48.94
	2	A5	P10	31	56	55.36
4	3	A1	P2	35	59	59.32
	1	A1	P2	34	99	34.34
	1	A3	P6	43	84	51.19
	2	A1	P2	48	78	61.54
	2	A3	P6	40	79	50.63
	2	A5	P10	29	85	34.12
5	3	A1	P2	35	93	37.63
	1	A1	P2	11	35	31.43
	2	A1	P2	23	43	53.49
	2	A3	P6	29	39	74.36
	3	A1	P2	24	33	72.72
	3	A3	P6	26	38	68.42

HPR high proliferation region, *ORR* overlap region rate

Table 2. The ORR of high proliferative region between PET and corresponding pathology image in 6f/12d

Tumor	Segment no.	PET layer no.	Path section no.	HPRpet ∩ HPRpath	HPRpet ∪ HPRpath	ORR (%)
1	1	A1	P2	29	50	58.00
	2	A1	P2	31	60	51.67
	2	A3	P6	32	61	52.46
	3	A1	P2	25	47	53.19
2	3	A3	P6	26	45	57.78
	1	A1	P2	35	57	61.40
	1	A3	P6	33	59	55.93
	2	A1	P2	38	61	62.30
	2	A3	P6	40	64	62.50
	3	A1	P2	37	60	61.67
3	3	A3	P6	28	48	58.33
	1	A1	P2	31	52	59.62
	2	A1	P2	33	53	62.26
	2	A3	P6	34	55	61.82
	2	A5	P10	29	50	58.00
4	3	A1	P2	26	48	54.17
	1	A1	P2	23	47	48.94
	1	A3	P6	31	49	63.27
	2	A1	P2	30	47	63.83
	2	A3	P6	27	44	61.36
	2	A5	P10	26	46	56.52
	3	A1	P2	24	51	47.06

HPR high proliferation region, ORR overlap region rate

tumors ($F=8.427$, $P=0.002$). In addition, there were similar ORRs in both A1 layers of PET imaging between segments 1 and 2 in each tumor (Table 2).

Discussion

Our results presented here complement those of previous studies demonstrating a potential role for [¹⁸F]FLT PET in real-time detection of repopulation during radiotherapy without addressing the issue of spatial correspondence between the patterns of FLT uptake and cellular proliferation. Accelerated repopulation of tumor cells occurs with prolonged overall radiotherapy treatment time has been demonstrated *via* a variety of experimental models [6, 7, 12, 13]. In the first set of our experiments, the SUVmax decreased in the 3f/6d group compared to the non-irradiated tumors. However, it significantly increased in the 6f/12d group later, and then gradually decreased with prolonged treatment time. Proliferation changes on pathology images at the 6f/12d group were also confirmed. Similar results were found in FaDu human squamous cell carcinoma (FaDu-hSCC) xenograft model, with tumor repopulation being induced by prolonging treatment time with every-second-day (rather than daily) irradiation schedules [10]. Different from our study, the time point of tumor repopulation was observed in the 12f/24d and 18f/36d groups. In the FaDu-hSCC xenograft model, tumor repopulation was elicited by prolonging treatment time with the 12f/24d and 18f/36d groups, comparing the daily irradiated group with 12f/12d and 18f/18d. In this study, all tumors were irradiated with every other day fraction. The trend of SUVmax in different groups was analyzed during irradiation. This difference in experimental design may explain the discordance between another study and ours. In fact, consideration of when the [¹⁸F]FLT PET imaging

surrogate should be used for evaluating proliferation during radiotherapy is very important. In this study, we determined the time point of the accelerated repopulation as the dose reached 6f/12d by serial PET/CT scans, whereas little clinical studies directly detected repopulation in humans.

Although less general diagnostic applications with [¹⁸F]FLT PET imaging in clinical practice, the issue of spatial concordance is of utmost importance in the planning of radiotherapy, since the pattern of uptake of the PET tracer could potentially determine the dose painting of sub-volumes to treat cancer patients. In previous studies, it was demonstrated that [¹⁸F]FLT uptake by the tumor as a whole (maximum or average SUV) correlates well with the Ki-67 LI in both experimental tumor models and patient tumor specimens [14–16]. Otherwise, [¹⁸F]FLT uptake can reflect the treatment responses during radical radiotherapy [17]. However, these validation studies did not evaluate the spatial co-localization between the pattern of FLT uptake and the biological markers of cell proliferation. Our study tried to use thin tissue autoradiography and microscopy to image the tumor microenvironment to demonstrate the co-localization between intratumoral PET tracer uptake and tumor microenvironmental markers. Significant correlations were found between the SUVmax and Ki-67 LI of all ROIs in each *in vitro* tumor of the cell proliferation group ($P<0.001$). Similar results were also found in the accelerated repopulation group ($P<0.001$). Although the nonparametric Spearman rank test can express the strength of a linear functional relationship between the pixel intensities of two co-registered images, but it is not the optimal way to measure the spatial co-localization of [¹⁸F]FLT PET tracer uptake and the cell proliferation from thin tissue specimens. Threshold-based approaches provide an alternative and a more intuitive approach to analyzing these two signals. Overlap analysis metrics can be

used to assess the spatial concordance of the segmented autoradiography and microscopy images. Therefore, the ORR was cited in our study to evaluate the relationship between the high uptake region in PET image and high proliferative area in the corresponding layer of even pathological specimens. We found that the mean ORRs were more than 50 % in all layers of the tumor cell proliferation and repopulation groups.

Furthermore, using the same exhibited lesion of crisscross passageway as reference, the ORRs in both A1 layers of PET imaging between segments 1 and 2 in each tumor were very close in these two groups. In addition, it was notable that we used an *ex vivo* model to investigate the uptake of [¹⁸F]FLT within the tumor in our study. Although both removal of the tumor and the slicing might influence tumor architecture, [¹⁸F]FLT dose not undergo further metabolism and is therefore trapped within the cell. The PET scanning of the surgical specimen may thus represent the situation *in vivo*. Moreover, we used an *in vitro* tumor-marker-holder to make sure the autoradiography and microscopy images were co-registered correctly.

Further studies should be held to explain the spatial concordance between the intratumoral pattern of [¹⁸F]FLT uptake and the spatial distribution of cell proliferation in human pathological samples, which imaging with this particular tracer could provide useful information on the spatial distribution of actively proliferating cell.

Conclusions

Within the limitations of our study, we demonstrated that [¹⁸F]FLT PET may have a potential role for *in vivo* monitoring of tumor cell proliferation and repopulation during fractionated radiotherapy. Furthermore, [¹⁸F]FLT is a promising surrogate of tumor proliferative response to fractionated radiotherapy which may help in adaptive radiation oncology treatment planning.

Acknowledgments. We would like to thank the Jiangsu Atomic Energy Laboratory for providing the micro-PET and micro-CT scanner. This result was presented as a poster discussion in the American Society for Radiation Oncology 59th Annual Meeting.

Funding Information This article is supported by the National Natural Science Foundation of China (81472810) and the Science and Technology Development Plans of Shandong Province (2014GSF118138, 2016GSF201099).

Compliance with Ethical Standards

Conflict of Interest Statement

None declared.

Ethics Statement

Animal maintenance and all experimental procedures were carried out according to the protocol approved by the Chinese animal welfare regulations.

Open Access This article is distributed under the terms of the Creative Commons Attribution 4.0 International License (<http://creativecommons.org/licenses/by/4.0/>), which permits unrestricted use, distribution, and reproduction in any medium, provided you give appropriate credit to the original author(s) and the source, provide a link to the Creative Commons license, and indicate if changes were made.

References

1. Chun SG, Hu C, Choy H, Komaki RU, Timmerman RD, Schild SE, Bogart JA, Dobelbower MC, Bosch W, Galvin JM, Kavadi VS, Narayan S, Iyengar P, Robinson CG, Wynn RB, Raben A, Augspurger ME, MacRae RM, Paulus R, Bradley JD (2017) Impact of intensity-modulated radiation therapy technique for locally advanced non-small cell lung cancer: a secondary analysis of the NRG oncology RTOG 0617 randomized clinical trial. *J Clin Oncol* 35:56–62
2. Brower JV, Amini A, Chen S, Hullett CR, Kimple RJ, Wojcieszynski AP, Bassetti M, Witek ME, Yu M, Harari PM, Baschnagel AM (2016) Improved survival with dose-escalated radiotherapy in stage III non-small-cell lung cancer: analysis of the national cancer database. *Ann Oncol* 27:1887–1894
3. Tucker SL, Liu A, Gomez D, Tang LL, Allen P, Yang J, Liao Z, Grosshans D (2016) Impact of heart and lung dose on early survival in patients with non-small cell lung cancer treated with chemoradiation. *Radiother Oncol* 119:495–500
4. Even AJ, van der Stoep J, Zegers CM et al (2015) PET-based dose painting in non-small cell lung cancer: comparing uniform dose escalation with boosting hypoxic and metabolically active subvolumes. *Radiother Oncol* 116:281–286
5. Liu J, Li C, Hu M, Lu J, Shi X, Xing L, Sun X, Fu Z, Yu J, Meng X (2015) Exploring spatial overlap of high-uptake regions derived from dual tracer positron emission tomography computer tomography imaging using ¹⁸F-fluorodeoxyglucose and ¹⁸F-fluorodeoxythymidine in non-small cell lung cancer patients: a prospective pilot study. *Medicine* 94:e678
6. Troost EG, Bussink J, Hoffmann AL et al (2010) ¹⁸F-FLT PET/CT for early response monitoring and dose escalation in oropharyngeal tumor. *J Nucl Med* 51:866–874
7. Fenwick JD, Pardo-Montero J, Nahum AE, Malik ZI (2012) Impact of schedule duration on head and neck radiotherapy: accelerated tumor repopulation versus compensatory mucosal proliferation. *Int J Radiat Oncol Biol Phys* 82:1021–1030
8. Baumann M, Herrmann T, Koch R, Matthiessen W, Appold S, Wahlers B, Kepka L, Marschke G, Feltl D, Fietkau R, Budach V, Dunst J, Dziadziszko R, Krause M, Zips D (2011) Final results of the randomized phase III CHARTWEL-trial (ARO 97-1) comparing hyperfractionated-accelerated versus conventionally fractionated radiotherapy in non-small cell lung cancer (NSCLC). *Radiother Oncol* 100:76–85
9. Axente M, He J, Bass CP, Hirsch JI, Sundaresan G, Zweit J, Pugachev A (2011) Comprehensive approach to coregistration of autoradiography and microscopy images acquired from a set of sequential tissue sections. *J Nucl Med* 52:1621–1629
10. Yue JB, Yang J, Liu J, Lee J, Cabrera AR, Sun XD, Bai GH, Li YH, Yu JM (2014) Histopathologic validation of 3'-deoxy-3'-¹⁸F-fluorothymidine PET for detecting tumor repopulation during fractionated radiotherapy of human FaDu squamous cell carcinoma in nude mice. *Radiother Oncol* 111:475–481
11. van Baardwijk A, Bosmans G et al (2008) Correlation of intra-tumor heterogeneity on ¹⁸F-FDG PET with pathologic features in non-small cell lung cancer: a feasibility study. *Radiother Oncol* 87:55–58
12. Fatema CN, Zhao S, Zhao Y, Murakami M, Yu W, Nishijima KI, Tamaki N, Kitagawa Y, Kuge Y (2013) Monitoring tumor proliferative response to radiotherapy using ¹⁸F-fluorothymidine in human head and neck cancer xenograft in comparison with Ki-67. *Ann Nucl Med* 27(4):355–362
13. Butof R, Baumann M (2013) Time in radiation oncology-keep it short! *Radiother Oncol* 106:271–275
14. Nedergaard MK, Michaelsen SR, Perryman L, Eler J, Poulsen HS, Stockhausen MT, Lassen U, Kjaer A (2016) Comparison of (18)F-FET and ¹⁸F-FLT small animal PET for the assessment of anti-VEGF

- treatment response in an orthotopic model of glioblastoma. *Nucl Med Biol* 43:198–205
15. Crippa F, Agresti R, Sandri M, Mariani G, Padovano B, Alessi A, Bianchi G, Bombardieri E, Maugeri I, Rampa M, Carcangiu ML, Trecate G, Pascali C, Bogni A, Martelli G, de Braud F (2015) ¹⁸F-FLT PET/CT as an imaging tool for early prediction of pathological response in patients with locally advanced breast cancer treated with neoadjuvant chemotherapy: a pilot study. *Eur J Nucl Med Mol Imaging* 42:818–830
 16. Perumal M, Stronach EA, Gabra H, Aboagye EO (2012) Evaluation of 2-deoxy-2-[¹⁸F]fluoro-D-glucose- and 3'-deoxy-3'-[¹⁸F]fluorothymidine-positron emission tomography as biomarkers of therapy response in platinum-resistant ovarian cancer. *Mol Imaging Biol* 14:753–761
 17. Everitt S, Hicks RJ, Ball D, Kron T, Schneider-Kolsky M, Walter T, Binns D, Mac Manus M (2009) Imaging cellular proliferation during chemoradiotherapy: a pilot study of serial ¹⁸F-FLT positron emission tomography/computed tomography imaging for non-small-cell lung cancer. *Int J Radiat Oncol Biol Phys* 75:1098–1104